

Beyond the isotropic-model approximation in the theory of thermal conductivity

M. Omini and A. Sparavigna

Dipartimento di Fisica, Politecnico di Torino, Corso Duca degli Abruzzi 24, I-10129 Torino, Italy

(Received 24 July 1995)

By the use of an iterative method the linearized phonon-Boltzmann equation for a dielectric solid subjected to a thermal gradient is solved in the frame of three-phonon interactions. In this way it is possible to calculate the thermal conductivity of rare-gas solids starting from the pair potential and accounting for the real Brillouin zone of the lattice. The numerical results are in full agreement with experiment and represent a considerable improvement with respect to those previously deduced for an isotropic solid.

I. INTRODUCTION

In a previous paper,¹ referred to as I, we outlined an iterative method to solve the linearized Boltzmann equation for a system of interacting particles subjected to an external field. With respect to the variational approach,²⁻⁶ where the answer is affected by the form adopted, generally without justification, for the trial function, the above method presents the advantage of being independent of any arbitrary assumption, apart from the obvious requirement that the iteration procedure must be convergent.

The reliability of the new method was checked in I with reference to an isotropic solid subjected to a thermal gradient. In this paper we will apply the same procedure to a real crystal (namely, to a rare-gas solid described by the real Brillouin zone) and obtain in this way the solution of the transport problem in the frame of three-phonon interactions. Although the numerical accuracy of the results is, in principle, limited by the tremendous amount of time and financial support required by the computer to perform the program connected with the evaluation of the successive iterations, nevertheless our calculations are sufficient to check the convergence of the iteration procedure and consequently the possibility of obtaining the true behavior of the phonon distribution function in the whole Brillouin zone. Moreover, since the convergence is found in the whole temperature range, our solution takes automatically into account, for any temperature, the real roles played by normal and umklapp processes, being completely independent of assumptions concerning the small ratio of the normal to the umklapp phonon mean free path, as conversely invoked in the perturbative approaches discussed by Gurzhi⁷ and Gurevich.⁸ For all these reasons we are led to believe that the iterative method outlined in I represents a suitable approach to the solution of the Boltzmann equation for any kind of transport problems.

II. THREE-PHONON SCATTERING PROCESSES IN A FCC LATTICE

Let h_1 be the nearest-neighbor distance in a fcc lattice and \mathbf{u}_i the unit vectors corresponding to Cartesian coordinates x_i ($i=1,2,3$), chosen along the sides of the periodic cube in the direct space. Measuring the components q_i of any vector \mathbf{q} in units of the size $d=2\pi\sqrt{2}/h_1$ of the periodic cube of the reciprocal lattice, namely putting $q_i=d\eta_i$, and introducing

cylindrical coordinates θ, η, ζ through the equations

$$\eta_1 = \eta \cos \theta, \quad \eta_2 = \eta \sin \theta, \quad \eta_3 = \zeta, \quad (1)$$

it is easy to deduce that the boundary of the first Brillouin zone (BZ) in the plane $\zeta=0$ is defined by the equations $\pm \eta_1 \pm \eta_2 = 3/4$ and $\pm \eta_1 = 1/2, \pm \eta_2 = 1/2$. In other words, with reference to Fig. 1, it is the octagonal path with equation $\eta_b = H(\theta)$, where η_b is the value of η corresponding to a point of the boundary and $H(\theta)$ the function represented in Table I.

If from a given point (θ, η) lying within the zone section $\zeta=0$, we move along a parallel to the ζ axis, we cross the boundary of the BZ at a point with $\zeta_b = \pm M(\theta, \eta)$, where M is defined as the minimum among the absolute values of ζ attributed to the above point by the equations $\pm \eta_1 \pm \eta_2 \pm \eta_3 = 3/4$ and $\pm \eta_3 = 1/2$: in other words,

$$M(\theta, \eta) = \min \left\{ \left| \frac{3}{4} \pm \eta \cos \theta \pm \eta \sin \theta \right|, \frac{1}{2} \right\}. \quad (2)$$

Let $V(r)$ be the pair potential describing the interaction between atoms of the crystal. Introducing the operator $O_r = r^{-1}d/dr$, we can write the eigenvalue equation for the phonon frequencies ω and polarization vectors \mathbf{e} in the form⁵

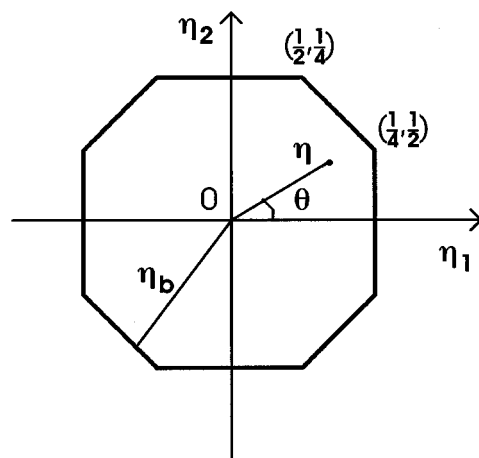


FIG. 1. Octagonal path describing the boundary of the BZ in the plane $\zeta=0$.

TABLE I. The function $H(\theta)$ describing the boundary of the BZ in the plane $\zeta=0$.

θ	$H(\theta)$
$0 \leq \theta \leq tg^{-1} \frac{1}{2}$	$\frac{1}{2 \cos \theta}$
$tg^{-1} \frac{1}{2} \leq \theta \leq tg^{-1} 2$	$\frac{3}{4(\cos \theta + \sin \theta)}$
$tg^{-1} 2 \leq \theta \leq \frac{\pi}{2} + tg^{-1} \frac{1}{2}$	$\frac{1}{2 \sin \theta}$
$\frac{\pi}{2} + tg^{-1} \frac{1}{2} \leq \theta \leq \pi - tg^{-1} \frac{1}{2}$	$\frac{1}{4(-\cos \theta + \sin \theta)}$
$\pi - tg^{-1} \frac{1}{2} \leq \theta \leq \pi + tg^{-1} \frac{1}{2}$	$-\frac{1}{2 \cos \theta}$
$\pi + tg^{-1} \frac{1}{2} \leq \theta \leq \frac{3}{2} \pi - tg^{-1} \frac{1}{2}$	$-\frac{1}{4(\cos \theta + \sin \theta)}$
$\frac{3}{2} \pi - tg^{-1} \frac{1}{2} \leq \theta \leq \frac{3}{2} \pi + tg^{-1} \frac{1}{2}$	$-\frac{1}{2 \sin \theta}$
$\frac{3}{2} \pi + tg^{-1} \frac{1}{2} \leq \theta \leq 2\pi - tg^{-1} \frac{1}{2}$	$\frac{1}{4(\cos \theta - \sin \theta)}$
$2\pi - tg^{-1} \frac{1}{2} \leq \theta \leq 2\pi$	$\frac{1}{2 \cos \theta}$

$$\sum_h (1 - \cos \mathbf{q} \cdot \mathbf{h}) [\gamma_h \mathbf{e} + \beta_h (\mathbf{h} \cdot \mathbf{e}) \mathbf{h}] = m \omega^2 \mathbf{e}, \quad (3)$$

where $\gamma_h = O_h V$, $\beta_h = O_h^2 V$ and m is the mass of each atom. With reference to a Lennard-Jones potential

$$V(r) = \Phi_0 \left[\left(\frac{r_0}{r} \right)^{12} - \left(\frac{r_0}{r} \right)^6 \right], \quad (4)$$

it is convenient to define dimensionless parameters $\sigma(h) = h_1^2 \Phi_0^{-1} \gamma_h$ and $\rho(h) = h_1^4 \Phi_0^{-1} \beta_h$. In this way, collecting together in the sum over \mathbf{h} the contributions coming from all the neighbors belonging to the same shell, we rewrite Eq. (3) as

$$\sum_s \sum_t (1 - \cos \mathbf{q} \cdot \mathbf{h}_t^s) \left[\sigma^s \mathbf{e} + \frac{\rho_s}{h_1^2} (\mathbf{h}_t^s \cdot \mathbf{e}) \mathbf{h}_t^s \right] = \frac{h_1^2 m \omega^2}{\Phi_0} \mathbf{e}, \quad (5)$$

where s runs over all the shells of neighbors, the position vector of the t th neighbor in the s th shell (of radius h_s) being denoted by \mathbf{h}_t^s , and $\sigma_s = \sigma(h_s)$, $\rho_s = \rho(h_s)$. It is easy to see⁹ that vectors \mathbf{h}_t^s can be written as linear combinations of the \mathbf{u}_i^s 's, in the form

$$\mathbf{h}_t^s = \frac{h_1}{\sqrt{2}} \sum_{i=1}^3 x_{ti}^s \mathbf{u}_i, \quad (6)$$

where $x_{t1}^s, x_{t2}^s, x_{t3}^s$ are of the form (1,1,0), (1,0,1),... for $s=1$ (first shell), (2,0,0), (0,2,0),... for $s=2$ (second shell), etc.

Defining the reduced frequencies

$$\bar{\omega} = h_1 \left(\frac{2m}{\Phi_0} \right)^{1/2} \omega, \quad (7)$$

and the dimensionless quantities

$$\Xi_t^s(\theta, \eta, \zeta) = 2\pi (\eta x_{t1}^s \cos \theta + \eta x_{t2}^s \sin \theta + \zeta x_{t3}^s), \quad (8)$$

$$T_{mn}(\theta, \eta, \zeta) = \sum_{s,t} (1 - \cos \Xi_t^s) (2\sigma_s \delta_{nm} + \rho_s x_{tm}^s x_{tn}^s), \quad (9)$$

one can easily reduce Eq. (5) to a linear homogeneous system for the three components e_1, e_2, e_3 of the vector \mathbf{e} , giving rise to the following algebraic equation for $\bar{\omega}$:

$$(T_{11} - \bar{\omega}^2) [(T_{22} - \bar{\omega}^2)(T_{33} - \bar{\omega}^2) - T_{23}^2] + T_{12} [T_{23} T_{13} - T_{12} (T_{33} - \bar{\omega}^2)] + T_{13} [T_{12} T_{23} - T_{13} (T_{22} - \bar{\omega}^2)] = 0. \quad (10)$$

For each of the three roots $\bar{\omega}_p$ of the above equation (defining the three branches of the phonon spectrum) we deduce the components of \mathbf{e}_p in the form

$$e_{p1} = [T_{12} T_{23} - T_{13} (T_{22} - \bar{\omega}_p^2)] / D_p, \quad (11)$$

$$e_{p2} = [T_{13} T_{12} - T_{23} (T_{11} - \bar{\omega}_p^2)] / D_p, \quad (12)$$

$$e_{p3} = [(T_{11} - \bar{\omega}_p^2)(T_{22} - \bar{\omega}_p^2) - T_{12}^2] / D_p, \quad (13)$$

where

$$D_p = \{ [T_{12} T_{23} - T_{13} (T_{22} - \bar{\omega}_p^2)]^2 + [T_{13} T_{12} - T_{23} (T_{11} - \bar{\omega}_p^2)]^2 + [(T_{11} - \bar{\omega}_p^2)(T_{22} - \bar{\omega}_p^2) - T_{12}^2]^2 \}^{1/2}. \quad (14)$$

Let us now consider a three-phonon scattering described by the conservation equations

$$\mathbf{q} \pm \mathbf{q}' = \mathbf{q}'' + \mathbf{g}, \quad (15)$$

$$\bar{\omega}_p(\mathbf{q}) \pm \bar{\omega}_{p'}(\mathbf{q}') - \bar{\omega}_{p''}(\mathbf{q}'') = 0, \quad (16)$$

where \mathbf{g} is a reciprocal-lattice vector and the upper and the lower sign refer to the processes $(\mathbf{q}p) + (\mathbf{q}'p') \rightarrow (\mathbf{q}''p'')$ and $(\mathbf{q}p) \rightarrow (\mathbf{q}'p') + (\mathbf{q}''p'')$, respectively. Expressing \mathbf{g} in terms of the \mathbf{u}_i^s 's (Ref. 9) and recalling Eq. (1) we rewrite Eq. (15) in the form

$$\eta_i \pm \eta'_i - \frac{1}{2} \mu_{ki}^{\nu} = \eta''_i, \quad (17)$$

where ν labels the shell of the reciprocal lattice, k the point of the reciprocal lattice belonging to this shell, and $\mu_{k1}^{\nu}, \mu_{k2}^{\nu}, \mu_{k3}^{\nu}$ are of the form (1,1,1), (-1,1,1),... for $\nu=1$ (first shell), (2,0,0), (0,2,0),... for $\nu=2$ (second shell), etc. The case $\nu=0$ corresponds to $\mathbf{g}=0$ (normal processes) and, consequently, $\mu_{ki}^{\nu}=0$.

For a given choice of (η_1, η_2) and (η'_1, η'_2) , that is of (η, θ) and (η', θ') , we easily deduce from Eq. (17) the length and the direction of vector $(\eta''_1 \mathbf{u}_1 + \eta''_2 \mathbf{u}_2)$, through the relations

$$\eta'' = \{ (\eta \cos \theta \pm \eta' \cos \theta' - \lambda_{k1}^{\nu})^2 + (\eta \sin \theta \pm \eta' \sin \theta' - \lambda_{k2}^{\nu})^2 \}^{1/2}, \quad (18)$$

$$\text{tg } \theta'' = \frac{\eta \sin \theta \pm \eta' \sin \theta' - \lambda_{k2}^{\nu}}{\eta \cos \theta \pm \eta' \cos \theta' - \lambda_{k1}^{\nu}}, \quad (19)$$

where $\lambda_{ki}^{\nu} = \mu_{ki}^{\nu}/2$ and θ'' belongs to the first, second, third, fourth quadrant, according to the conditions (1) $D>0, N>0$; (2) $D<0, N>0$; (3) $D<0, N<0$; (4) $D>0, N<0$, respec-

tively, N and D being the numerator and the denominator of the fraction appearing in Eq. (19).

Hereafter we will use the notation $\omega_p(\theta, \eta, \zeta)$ to indicate the angular frequency of the p th branch corresponding to the vector \mathbf{q} specified by the cylindrical coordinates θ, η, ζ . In this way from Eq. (16), owing to Eq. (17) written for $i=3$, we deduce

$$\bar{\omega}_p(\theta, \eta, \zeta) \pm \bar{\omega}_{p'}(\theta', \eta', \zeta') = \bar{\omega}_{p''}(\theta'', \eta'', \zeta \pm \zeta' - \lambda_{k3}^v). \quad (20)$$

Expressing θ' and η' with the help of Eqs. (18) and (19) we see that Eq. (20) represents an equation to be solved for ζ' . The j th solution of Eq. (20) satisfying the condition

$$-M(\theta', \eta') \leq \zeta' \leq M(\theta', \eta') \quad (21)$$

will simply be denoted by $\zeta'_\pm(j)$: it obviously depends on the variables $\theta, \eta, \zeta, \theta', \eta'$ and on the indices ν, k, p, p', p'' . Correspondingly we will denote by $\zeta''_\pm(j)$ the quantities $\zeta \pm \zeta'_\pm(j) - \lambda_{k3}^v$.

III. TRANSPORT EQUATION FOR THE PHONON SYSTEM UNDER A THERMAL GRADIENT

The linearized Boltzmann equation for a solid subjected to a thermal gradient can be written in the form^{2,3}

$$\begin{aligned} k_B T \mathbf{v}_{\mathbf{q}p} \cdot \nabla T \frac{\partial n_{\mathbf{q}p}^0}{\partial T} \\ = \sum_{\mathbf{q}'p'} \sum_{\mathbf{q}''p''} Q_{\mathbf{q}p, \mathbf{q}'p'}^{\mathbf{q}''p''} [\Psi_{\mathbf{q}''p''} - \Psi_{\mathbf{q}'p'} - \Psi_{\mathbf{q}p}] \\ + \frac{1}{2} \sum_{\mathbf{q}'p'} \sum_{\mathbf{q}''p''} Q_{\mathbf{q}p}^{\mathbf{q}'p', \mathbf{q}''p''} [\Psi_{\mathbf{q}''p''} + \Psi_{\mathbf{q}'p'} - \Psi_{\mathbf{q}p}], \end{aligned} \quad (22)$$

where the deviation function $\Psi_{\mathbf{q}p}$ is defined in terms of the perturbed and unperturbed phonon distributions $n_{\mathbf{q}p}$ and $n_{\mathbf{q}p}^0$ respectively, according to the equation

$$n_{\mathbf{q}p} = n_{\mathbf{q}p}^0 - \Psi_{\mathbf{q}p} \frac{\partial n_{\mathbf{q}p}^0}{\partial(\hbar \omega_{\mathbf{q}p})}. \quad (23)$$

The probability rates for the phonon processes $(\mathbf{q}p) + (\mathbf{q}'p') \rightarrow (\mathbf{q}''p'')$ and $(\mathbf{q}p) \rightarrow (\mathbf{q}'p') + (\mathbf{q}''p'')$ are given by

$$\begin{aligned} Q_{\mathbf{q}p, \mathbf{q}'p'}^{\mathbf{q}''p''} = \frac{\pi \hbar}{16m^3 N} \frac{n_{\mathbf{q}p}^0 n_{\mathbf{q}'p'}^0 (1 + n_{\mathbf{q}''p''}^0)}{\omega_{\mathbf{q}p} \omega_{\mathbf{q}'p'} \omega_{\mathbf{q}''p''}} \delta(\omega_{\mathbf{q}p} + \omega_{\mathbf{q}'p'} \\ - \omega_{\mathbf{q}''p''}) \mathcal{R}_{\mathbf{q}p, \mathbf{q}'p', \mathbf{q}''p''}^+ \end{aligned} \quad (24)$$

and

$$\begin{aligned} Q_{\mathbf{q}p}^{\mathbf{q}'p', \mathbf{q}''p''} = \frac{\pi \hbar}{16m^3 N} \frac{n_{\mathbf{q}p}^0 (1 + n_{\mathbf{q}'p'}^0) (1 + n_{\mathbf{q}''p''}^0)}{\omega_{\mathbf{q}p} \omega_{\mathbf{q}'p'} \omega_{\mathbf{q}''p''}} \delta(\omega_{\mathbf{q}p} - \omega_{\mathbf{q}'p'} \\ - \omega_{\mathbf{q}''p''}) \mathcal{R}_{\mathbf{q}p, \mathbf{q}'p', \mathbf{q}''p''}^- \end{aligned} \quad (25)$$

respectively, N being the total number of atoms in the crystal and the factors \mathcal{R}^\pm depending on the polarization vectors through the expression (see I)

$$\begin{aligned} \mathcal{R}_{\mathbf{q}p, \mathbf{q}'p', \mathbf{q}''p''}^\pm = \left| \sum_{\mathbf{h}} \{ \alpha_{\mathbf{h}} (\mathbf{h} \cdot \mathbf{e}_{\mathbf{q}p}) (\mathbf{h} \cdot \mathbf{e}_{\mathbf{q}'p'}) (\mathbf{h} \cdot \mathbf{e}_{\mathbf{q}''p''}) + \beta_{\mathbf{h}} [(\mathbf{h} \cdot \mathbf{e}_{\mathbf{q}p}) (\mathbf{e}_{\mathbf{q}'p'} \cdot \mathbf{e}_{\mathbf{q}''p''}) + (\mathbf{h} \cdot \mathbf{e}_{\mathbf{q}'p'}) (\mathbf{e}_{\mathbf{q}p} \cdot \mathbf{e}_{\mathbf{q}''p''}) \right. \\ \left. + (\mathbf{h} \cdot \mathbf{e}_{\mathbf{q}''p''}) (\mathbf{e}_{\mathbf{q}p} \cdot \mathbf{e}_{\mathbf{q}'p'}) \} \} (e^{i\mathbf{q} \cdot \mathbf{h}} - 1) (e^{\pm i\mathbf{q}' \cdot \mathbf{h}} - 1) (e^{-i\mathbf{q}'' \cdot \mathbf{h}} - 1) \right|^2, \end{aligned} \quad (26)$$

where $\alpha_{\mathbf{h}} = O_h^3 V$.

As in Eq. (5), it is convenient to transform the sum over \mathbf{h} into a sum over all the shells of neighbors. For the s th shell we define the reduced radius $\xi_s = h_s/h_1$ where $h_s = (h_1/\sqrt{2}) [(x_{i1}^s)^2 + (x_{i2}^s)^2 + (x_{i3}^s)^2]^{1/2}$, and the dimensionless parameter $\epsilon_s = -h_1^2 \xi_s^2 \alpha_s / \rho_s$, with $\alpha_s = \alpha(h_s)$. Owing to Eqs. (6) and (26) we easily obtain

$$\mathcal{R}^\pm = \frac{2\Phi_0^2}{h_1^6} |F^\pm|^2, \quad (27)$$

where

$$\begin{aligned} F^\pm = \sum_s \sum_t \left\{ -\frac{1}{2} \frac{\epsilon_s \rho_s}{\xi_s^2} (\mathbf{x}_t^s \cdot \mathbf{e}_p) (\mathbf{x}_t^s \cdot \mathbf{e}_{p'}) (\mathbf{x}_t^s \cdot \mathbf{e}_{p''}) + \rho_s [(\mathbf{x}_t^s \cdot \mathbf{e}_p) (\mathbf{e}_{p'} \cdot \mathbf{e}_{p''}) + (\mathbf{x}_t^s \cdot \mathbf{e}_{p'}) (\mathbf{e}_p \cdot \mathbf{e}_{p''}) + (\mathbf{x}_t^s \cdot \mathbf{e}_{p''}) (\mathbf{e}_p \cdot \mathbf{e}_{p'})] \right\} \\ \times \{ \sin(\Xi_t^s \pm \Xi_t'^s) - \sin \Xi_t^s \mp \sin \Xi_t'^s \}, \end{aligned} \quad (28)$$

having written $\mathbf{x}_t^s \cdot \mathbf{e}_p = x_{t1}^s e_{p1} + x_{t2}^s e_{p2} + x_{t3}^s e_{p3}$, etc., and $\Xi_t^s = \Xi_t^s(\theta, \eta, \zeta)$, $\Xi_t'^s = \Xi_t^s(\theta', \eta', \zeta')$.

Let us examine the right-hand side (rhs) of Eq. (22). One can transform the sum over \mathbf{q}'' into a sum over the reciprocal-lattice vectors \mathbf{g} (that is, over ν, k) using the momentum conservation condition (15). Conversely, the sums over \mathbf{q}' are amenable to integrals over the BZ by the help of the substitution

$$\sum_{\mathbf{q}'} \rightarrow \frac{\Omega}{(2\pi)^3} \int d^3\mathbf{q}' = \frac{\Omega}{(2\pi)^3} \left(\frac{2\pi\sqrt{2}}{h_1} \right)^3 \int_0^{2\pi} d\theta' \int_0^{H(\theta')} \eta' d\eta' \int_{-M(\eta',\theta')}^{M(\eta',\theta')} d\xi', \quad (29)$$

where Ω is the crystal volume. The presence of the δ functions appearing in Eqs. (24) and (25) eliminates the integration over ξ' , so that, setting $v = \Omega/N$ (lattice cell volume), one obtains

$$\begin{aligned} \text{rhs of Eq. (22)} &= \frac{v\pi\hbar\sqrt{2}}{mh_1^5} \left[\sum_{\nu,k} \sum_{p',p''} \int_0^{2\pi} d\theta' \int_0^{H(\theta')} \eta' d\eta' \right. \\ &\quad \times \sum_j \left\{ \frac{n^0 n^{0'} (1+n^{0''})}{\bar{\omega}\bar{\omega}'\bar{\omega}''} |F^+|^2 (\Psi'' - \Psi' - \Psi) \left| \frac{\partial\bar{\omega}'}{\partial\xi'} - \frac{\partial\bar{\omega}''}{\partial\xi''} \right|^{-1} \right\}_{\xi'=\xi'_+(j); \xi''=\xi''_+(j)} \\ &\quad + \frac{1}{2} \sum_{\nu,k} \sum_{p',p''} \int_0^{2\pi} d\theta' \int_0^{H(\theta')} \eta' d\eta' \sum_j \left\{ \frac{n^0 (1+n^{0'}) (1+n^{0''})}{\bar{\omega}\bar{\omega}'\bar{\omega}''} \right. \\ &\quad \left. \times \left| F^- \right|^2 (\Psi'' + \Psi' - \Psi) \left| \frac{\partial\bar{\omega}'}{\partial\xi'} - \frac{\partial\bar{\omega}''}{\partial\xi''} \right|^{-1} \right\}_{\xi'=\xi'_-(j); \xi''=\xi''_-(j)} \Big], \quad (30) \end{aligned}$$

where for each of the three functions $\Psi, \bar{\omega}, n^0$ we have used the compact notations $\Psi_p(\theta, \eta, \xi) = \Psi$, $\Psi_{p'}(\theta', \eta', \xi') = \Psi'$, $\Psi_{p''}(\theta'', \eta'', \xi'') = \Psi''$, and so on.

Since now $\mathbf{v}_{\mathbf{q}p} = \partial\omega_{\mathbf{q}p}/\partial\mathbf{q}$ we have, from Eq. (7),

$$\text{lhs of Eq. (22)} = \frac{k_B T}{4\pi} \left(\frac{\Phi_0}{m} \right)^{1/2} \frac{\partial n_p^0}{\partial T} \sum_i \frac{\partial \bar{\omega}_p}{\partial \eta_i} \left(\frac{\partial T}{\partial x_i} \right) \quad (31)$$

or also, from Eqs. (1) and (10)

$$\text{lhs of Eq. (22)} = \frac{k_B}{4\pi} \left(\frac{\Phi_0}{m} \right)^{1/2} b \bar{\omega}_p \frac{e^{b\bar{\omega}_p}}{(e^{b\bar{\omega}_p} - 1)^2} \sum_i A_{pi} \left(\frac{\partial T}{\partial x_i} \right), \quad (32)$$

where

$$b = \frac{\hbar}{h_1 k_B T} \left(\frac{\Phi_0}{2m} \right)^{1/2}, \quad (33)$$

$$\begin{aligned} A_{pi}(\theta, \eta, \xi) &= \frac{1}{B_p} \{ [(T_{22} - \bar{\omega}_p^2)(T_{33} - \bar{\omega}_p^2) - T_{23}^2] N_{11,i} + [(T_{11} - \bar{\omega}_p^2)(T_{33} - \bar{\omega}_p^2) - T_{13}^2] N_{22,i} + [(T_{11} - \bar{\omega}_p^2)(T_{22} - \bar{\omega}_p^2) - T_{12}^2] N_{33,i} \\ &\quad + 2[T_{12}T_{13} - T_{23}(T_{11} - \bar{\omega}_p^2)] N_{23,i} + 2[T_{23}T_{13} - T_{12}(T_{33} - \bar{\omega}_p^2)] N_{12,i} + 2[T_{12}T_{23} - T_{13}(T_{22} - \bar{\omega}_p^2)] N_{13,i} \}, \quad (34) \end{aligned}$$

$$N_{mn,i} = 2\pi \sum_{s,t} (\sin \Xi_t^s) (2\sigma_s \delta_{mn} + \rho_s x_{tm}^s x_{tn}^s) x_{ti}^s, \quad (35)$$

$$B_p = 2\bar{\omega}_p [3\bar{\omega}_p^4 - 2(T_{11} + T_{22} + T_{33})\bar{\omega}_p^2 - (T_{12}^2 + T_{23}^2 + T_{13}^2 - T_{11}T_{22} - T_{11}T_{33} - T_{22}T_{33})]. \quad (36)$$

Equating (30) to (31) and setting

$$\Psi_{\mathbf{q}p} = -\frac{\Phi_0 h_1^4}{8\pi^2 v T} f_p(\theta, \eta, \xi), \quad (37)$$

$$\bar{\omega}_p \frac{e^{b\bar{\omega}_p}}{(e^{b\bar{\omega}_p} - 1)^2} A_{pm} = \theta_{pm}(\theta, \eta, \xi), \quad (38)$$

$$\left\{ \frac{|F^\pm|^2}{|A_{p'3}(\theta', \eta', \zeta') - A_{p''3}(\theta'', \eta'', \zeta'')|} \right\}_{\zeta' = \zeta'_\pm(j); \zeta'' = \zeta''_\pm(j)} = K_{p', p'', j}^\pm(\theta, \eta, \zeta; \theta', \eta'), \tag{39}$$

we obtain

$$\begin{aligned} f_p(\theta, \eta, \zeta) &= \frac{1}{Q_p} \left[\theta_{p1} \left(\frac{\partial T}{\partial x_1} \right) + \theta_{p2} \left(\frac{\partial T}{\partial x_2} \right) + \theta_{p3} \left(\frac{\partial T}{\partial x_3} \right) \right] \\ &+ \frac{1}{Q_p} \sum_{v,k} \sum_{p'p''} \int_0^{2\pi} d\theta' \int_0^{H(\theta')} \eta' d\eta' \sum_j \left\{ \frac{n_p^0(\theta, \eta, \zeta) n_{p'}^0(\theta', \eta', \zeta') [1 + n_{p''}^0(\theta'', \eta'', \zeta'')]}{\bar{\omega}_p(\theta, \eta, \zeta) \bar{\omega}_{p'}(\theta', \eta', \zeta') \bar{\omega}_{p''}(\theta'', \eta'', \zeta'')} [f_{p''}(\theta'', \eta'', \zeta'') \right. \\ &\left. - f_{p'}(\theta', \eta', \zeta')] \right\}_{\zeta' = \zeta'_+(j); \zeta'' = \zeta''_+(j)} K_{p'p'', j}^+ \\ &+ \frac{1}{2Q_p} \sum_{v,k} \sum_{p'p''} \int_0^{2\pi} d\theta' \int_0^{H(\theta')} \eta' d\eta' \sum_j \left\{ \frac{n_p^0(\theta, \eta, \zeta) [1 + n_{p'}^0(\theta', \eta', \zeta')] [1 + n_{p''}^0(\theta'', \eta'', \zeta'')]}{\bar{\omega}_p(\theta, \eta, \zeta) \bar{\omega}_{p'}(\theta', \eta', \zeta') \bar{\omega}_{p''}(\theta'', \eta'', \zeta'')} \right. \\ &\left. \times [f_{p''}(\theta'', \eta'', \zeta'') + f_{p'}(\theta', \eta', \zeta')] \right\}_{\zeta' = \zeta'_-(j); \zeta'' = \zeta''_-(j)} K_{p'p'', j}^- \end{aligned} \tag{40}$$

where

$$\begin{aligned} Q_p(\theta, \eta, \zeta) &= \sum_{v,k} \sum_{p'p''} \int_0^{2\pi} d\theta' \int_0^{H(\theta')} \eta' d\eta' \sum_j \left\{ \frac{n_p^0(\theta, \eta, \zeta) n_{p'}^0(\theta', \eta', \zeta') [1 + n_{p''}^0(\theta'', \eta'', \zeta'')]}{\bar{\omega}_p(\theta, \eta, \zeta) \bar{\omega}_{p'}(\theta', \eta', \zeta') \bar{\omega}_{p''}(\theta'', \eta'', \zeta'')} \right\}_{\zeta' = \zeta'_+(j); \zeta'' = \zeta''_+(j)} K_{p'p'', j}^+ \\ &+ \frac{1}{2} \sum_{v,k} \sum_{p'p''} \int_0^{2\pi} d\theta' \int_0^{H(\theta')} \eta' d\eta' \sum_j \\ &\times \left\{ \frac{n_p^0(\theta, \eta, \zeta) [1 + n_{p'}^0(\theta', \eta', \zeta')] [1 + n_{p''}^0(\theta'', \eta'', \zeta'')]}{\bar{\omega}_p(\theta, \eta, \zeta) \bar{\omega}_{p'}(\theta', \eta', \zeta') \bar{\omega}_{p''}(\theta'', \eta'', \zeta'')} \right\}_{\zeta' = \zeta'_-(j); \zeta'' = \zeta''_-(j)} K_{p'p'', j}^- \end{aligned} \tag{41}$$

Equation (40) is precisely of the form of Eq. (11) in I and consequently can be solved through an iteration procedure. The solution is seen to be

$$f_p = \sum_i \mathcal{F}_{pi} \left(\frac{\partial T}{\partial x_i} \right), \tag{42}$$

where \mathcal{F}_{pi} is the limit for $n \rightarrow \infty$ of the functions \mathcal{F}_{pi}^n generated by the recurrence relation

$$\begin{aligned} \mathcal{F}_{pi}^{n+1} &= \frac{1}{Q_p} \theta_{pi} + \frac{1}{Q_p} \sum_{v,k} \sum_{p'p''} \int_0^{2\pi} d\theta' \int_0^{H(\theta')} \eta' d\eta' \sum_j \left\{ \frac{n_p^0(\theta, \eta, \zeta) n_{p'}^0(\theta', \eta', \zeta') [1 + n_{p''}^0(\theta'', \eta'', \zeta'')]}{\bar{\omega}_p(\theta, \eta, \zeta) \bar{\omega}_{p'}(\theta', \eta', \zeta') \bar{\omega}_{p''}(\theta'', \eta'', \zeta'')} [\mathcal{F}_{p''i}^n(\theta'', \eta'', \zeta'') \right. \\ &\left. - \mathcal{F}_{p'i}^n(\theta', \eta', \zeta')] \right\}_{\zeta' = \zeta'_+(j); \zeta'' = \zeta''_+(j)} K_{p'p'', j}^+ \\ &+ \frac{1}{2Q_p} \sum_{v,k} \sum_{p'p''} \int_0^{2\pi} d\theta' \int_0^{H(\theta')} \eta' d\eta' \sum_j \left\{ \frac{n_p^0(\theta, \eta, \zeta) [1 + n_{p'}^0(\theta', \eta', \zeta')] [1 + n_{p''}^0(\theta'', \eta'', \zeta'')]}{\bar{\omega}_p(\theta, \eta, \zeta) \bar{\omega}_{p'}(\theta', \eta', \zeta') \bar{\omega}_{p''}(\theta'', \eta'', \zeta'')} [\mathcal{F}_{p''i}^n(\theta'', \eta'', \zeta'') \right. \\ &\left. + \mathcal{F}_{p'i}^n(\theta', \eta', \zeta')] \right\}_{\zeta' = \zeta'_-(j); \zeta'' = \zeta''_-(j)} K_{p'p'', j}^- \end{aligned} \tag{43}$$

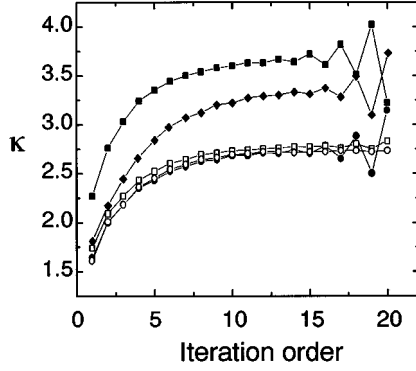


FIG. 2. Theoretical conductivity (in $\text{mW cm}^{-1} \text{K}^{-1}$) for argon at 80 K, evaluated in the nearest-neighbor approximation, as a function of the order of iteration for different choices of the number \mathcal{N} of points used to sample the Brillouin zone: $\mathcal{N}=2304$ (■), $\mathcal{N}=3240$ (◆), $\mathcal{N}=4400$ (●), $\mathcal{N}=7488$ (□), and $\mathcal{N}=11760$ (○).

IV. EXPRESSION OF THERMAL CONDUCTIVITY AND COMPARISON BETWEEN THEORY AND EXPERIMENT

The heat current density

$$\mathbf{U} = \frac{1}{\Omega} \sum_{\mathbf{q}\mathbf{p}} \hbar \omega_{\mathbf{q}\mathbf{p}} \mathbf{v}_{\mathbf{q}\mathbf{p}} n_{\mathbf{q}\mathbf{p}} = - \frac{1}{\Omega} \sum_{\mathbf{q}\mathbf{p}} \hbar \omega_{\mathbf{q}\mathbf{p}} \mathbf{v}_{\mathbf{q}\mathbf{p}} \frac{\partial n_{\mathbf{q}\mathbf{p}}^0}{\partial (\hbar \omega_{\mathbf{q}\mathbf{p}})} \Psi_{\mathbf{q}\mathbf{p}} \quad (44)$$

can now be easily evaluated by the help of (29), (37), and (42). One obtains the following expression for the n th component of \mathbf{U} with respect to the Cartesian reference system with unit vectors \mathbf{u}_i :

$$U_n = - \sum_i \kappa_{ni} \frac{\partial T}{\partial x_i}, \quad (45)$$

where

$$\begin{aligned} \kappa_{ni} &= \frac{\hbar \Phi_0^2}{16\pi^3 m v k_B T^2} \sum_p \int_0^{2\pi} d\theta \int_0^{H(\theta)} \eta d\eta \\ &\times \int_{-M(\theta, \eta)}^{M(\theta, \eta)} d\zeta \frac{e^{b\bar{\omega}_p}}{(e^{b\bar{\omega}_p} - 1)^2} \bar{\omega}_p A_{pn} \mathcal{F}_{pi}. \end{aligned} \quad (46)$$

As already anticipated in the Introduction, the main obstacle to the application of the theory developed in the previous sections is the time required by the computer to evaluate with a sufficient degree of accuracy the functions involved in each step of the iteration process. The problem is connected with the number of points one can use to sample the BZ in order to perform the multiple integrations: this number must be sufficiently high to allow the substitution of each integral by a sum over a finite number of terms, but, on the other hand, not so high to prevent us from arriving in an acceptable time at the convergence of the iteration procedure. A criterion for a reasonable choice is suggested in Fig. 2: here we consider, for the sake of simplicity, the ideal case where the interaction between argon atoms at 80 K is confined to nearest neighbors ($s=1$) and bring the theoretical conductivity vs the order of iteration, for various choices of the num-

TABLE II. Parameters of the interatomic potential as deduced from Wallace (Ref. 9).

Solid	Φ_0 (10^{-13} erg)	r_0 (Å)
Ar	0.583 56	3.4447
Kr	0.900 96	3.6621

ber of points (\mathcal{N}) used to sample the BZ. The choice $\mathcal{N}=2304$ is clearly unsatisfactory: it produces to undue oscillations of the curve for high orders of iteration, showing that a low density of points gives rise to numerical instability during the iteration procedure. This is understandable, since we start with the evaluation of $\mathcal{F}_{pi}^0 = \theta_{pi}/Q_p$ [see Eq. (43)] in the limited number of points corresponding to our sample: on the other hand, the integral required by Eq. (43) to obtain \mathcal{F}_{pi}^1 implies the knowledge of \mathcal{F}_{pi}^0 in the whole BZ [in particular, $\zeta'_\pm(j)$ and $\zeta''_\pm(j)$, as resulting from the solution of the energy and momentum conservation equations, correspond to point which are not necessarily included in the sample]. The numerical integration is performed by assigning to each point the value of \mathcal{F}_{pi}^0 pertaining to the closest point of the sample. Clearly, such an approximation gives rise to errors which affect \mathcal{F}_{pi}^1 , and can be amplified by the successive iterations. The resulting numerical instability deprives of any meaning the apparent saturation of the curve for iteration orders lower than ~ 15 . However, by inspection of the figure one notes that the above oscillations are progressively reduced and finally disappear for increasing values of \mathcal{N} : moreover, the asymptotic values corresponding to different choices of \mathcal{N} become undistinguishable when \mathcal{N} is large. This is interpreted as a good argument in favor of the choice $\mathcal{N}=7488$, which will be considered in the following (that is, in the real case where the interaction between atoms is extended to all the effective neighbors) as an acceptable compromise between the two different exigencies previously discussed.

In the frame of this choice we applied our method of solution to solid argon and krypton, extending the Lennard-Jones interaction up to the third shell of neighbors and accounting for scattering processes referring to $\nu=0$ (normal processes) and $\nu=1$ (umklapp processes). In fact we checked, on one hand, the negligible role played by the interaction terms connected with the fourth shell of neighbors; on the other hand, the absence of any contribution from processes with $\nu \geq 2$ (that is, from vectors \mathbf{g} pertaining to the second, third, ... shell of the reciprocal lattice). The parameters Φ_0 and r_0 entering the pair potential were deduced from Wallace⁹ and are reproduced in Table II.

A first important result of our calculation is the possibility of investigating the behavior of the deviation function along any given direction emerging from the origin of the BZ. Writing

$$\Psi_{\mathbf{q}\mathbf{p}} = -k_B h_1 F_p(\mathbf{q}) \left(\frac{\mathbf{q}}{|\mathbf{q}|} \cdot \nabla T \right), \quad (47)$$

we have, in the particular case with ∇T parallel to x_3 axis

$$\Psi_{\mathbf{q}\mathbf{p}} = -k_B h_1 F_p(\mathbf{q}) \left(\frac{\partial T}{\partial x_3} \right) \cos \alpha, \quad (48)$$

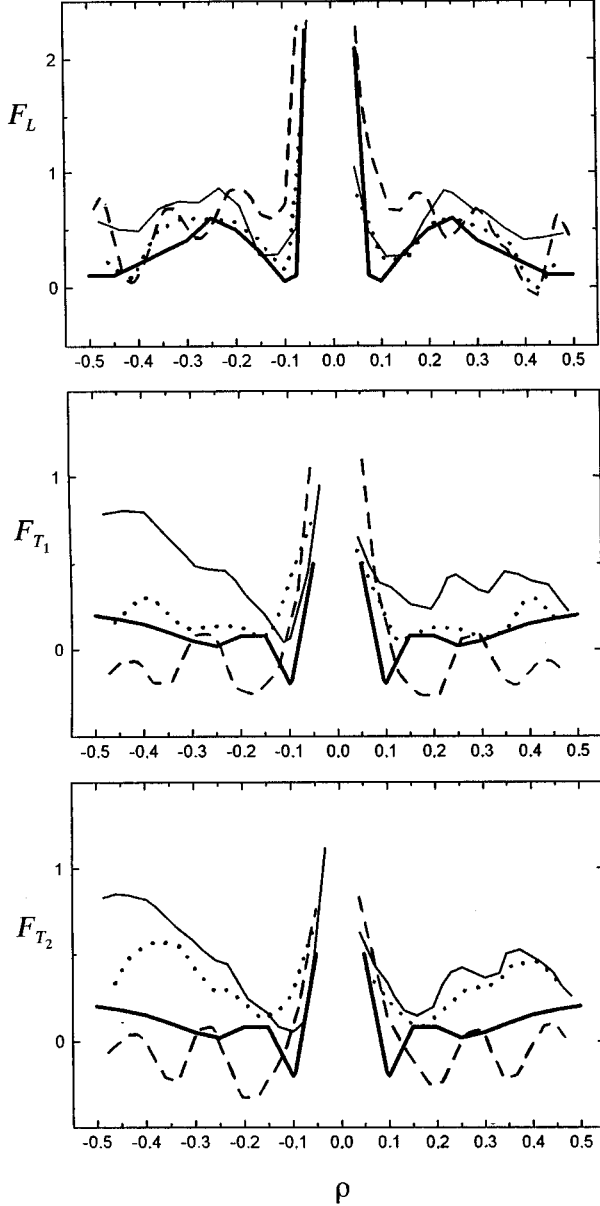


FIG. 3. Behavior of functions F_L , F_{T_1} and F_{T_2} in the plane $\theta=0$, as a function of the radial coordinate ρ , the temperature gradient being along the x_3 axis. The continuous thin line refers to $\alpha=0$, the dotted line to $\alpha=\pi/4$ and the dashed line to $\alpha=\pi/2$. The behavior of the corresponding functions evaluated by means of the isotropic model is represented by the continuous thick line.

where α is the angle of the selected direction (\mathbf{q}) with the x_3 axis. The second angle specifying this direction is, of course, the angle θ previously introduced in the plane $\zeta=0$. Equating expression (48) to (37) and accounting for (42), we deduce (from the relation $v=h_1^3/\sqrt{2}$)

$$F_p(\mathbf{q}) \equiv F_p(\theta, \alpha; \rho) = \frac{\Phi_0 \sqrt{2}}{8 \pi^2 k_B T \cos \alpha} \mathcal{F}_{p3}(\theta, \eta, \zeta), \quad (49)$$

where $\eta = \rho \sin \alpha$, $\zeta = \rho \cos \alpha$, ρ being the radial coordinate along the specified direction in units of d . Figure 3 reproduces the behaviors of functions F_p for $\theta=0$ and different

values of α , as deducible for Ar at 80 K from the 12th step of the iteration process. Analogous curves are obtained for other values of θ . The range $(0, \rho_{\max})$ for the allowed values of ρ changes with the direction, ρ_{\max} representing the reduced distance from the origin of the zone boundary along the direction itself. We notice that for a given α , the case corresponding to $\alpha + \pi$, that is to $\eta = -\rho \sin \alpha$, $\zeta = -\rho \cos \alpha$, can formally be obtained by leaving α unchanged and changing ρ into $-\rho$, so that it is exactly described by function (49) when this is interpreted as an analytical function of ρ in the range where ρ is negative. Consequently the two cases corresponding to α and $\alpha + \pi$ are automatically included in the same figure when the analytical function (49) is brought vs ρ in the whole range $-\rho_{\max} \leq \rho \leq \rho_{\max}$. It has also to be pointed out that when \mathbf{q} approaches the direction lying in the plane $\zeta=0$ (normal to ∇T) the denominator of function (49) goes to zero because in this case $\alpha \rightarrow \pi/2$, but also the numerator vanishes: in fact $A_{p3} \rightarrow 0$ for $\zeta \rightarrow 0$ and consequently, owing to Eqs. (38) and (43), \mathcal{F}_{p3} vanishes at any step of the iteration process. As a result the function $\mathcal{F}_{p3}/\cos \alpha$ must be substituted by

$$\rho \lim_{\zeta \rightarrow 0} \frac{\mathcal{F}_{p3}(\theta, \rho, \zeta)}{\zeta},$$

which has the symmetric behavior corresponding to the dashed curve of Fig. 3. The thick curves reproduce the predictions of the isotropic model, as deducible from the calculation performed in I (in this case the range of $|\rho|$ is extended from 0 to $Q_D/d=0.492$, Q_D being the radius of the Debye sphere). We notice the different scales used for longitudinal and transverse-branch diagrams, showing that the deviation from the equilibrium distribution is especially important for longitudinal branches.

The numerical evaluation of expressions (46), as obtained by leading the iteration process up to the 12th step, confirms, as expected, that tensor κ_{ni} is isotropic, that is $\kappa_{ni} = \kappa \delta_{ni}$ where κ can be interpreted as the thermal conductivity of the crystal. The reason for which the off-diagonal components vanish is related to the behavior of functions $A_{pn}(\theta, \eta, \zeta)$ and $\mathcal{F}_{pi}(\theta, \eta, \zeta)$ as a consequence of a 180° rotation around a coordinate axis: for instance, a rotation of this kind around the x_3 axis implies $A_{p1} \rightarrow -A_{p1}$, $A_{p2} \rightarrow -A_{p2}$, $A_{p3} \rightarrow A_{p3}$, while $\mathcal{F}_{p3} \rightarrow \mathcal{F}_{p3}$, so that any product $A_{pn} \mathcal{F}_{p3}$ with $n \neq 3$ is an odd function with respect to the transformation $\theta \rightarrow \theta + \pi$, $\eta \rightarrow \eta$, $\zeta \rightarrow \zeta$ and the corresponding integral in Eq. (46) (or in other words, κ_{n3}) is zero. Similar arguments, when applied to 180° rotations around the x_1 and x_2 axis, would lead to the conclusion that also κ_{n1} and κ_{n2} are zero, for $n \neq 1$ and $n \neq 2$, respectively. The equality of the diagonal components ($\kappa_{11} = \kappa_{22} = \kappa_{33}$) follows from the fact that the three coordinate axes are perfectly equivalent from the point of view of crystal symmetry: however, the numerical check of this equality is not obvious at all, since in some way the use of cylindrical coordinates in our calculation amounts to introducing a preferential direction (the x_3 axis) and consequently the three axes are not treated in the same way. In more specific terms, the volume element $\eta d\eta d\theta d\zeta$ does not contain the three variables η_1, η_2, η_3 in a symmetric way. Such a dissymmetry must obviously be immaterial when the density of points used to sample the BZ is very high, since the value

TABLE III. Ratio $(\kappa_{33}-\kappa_{11})/\kappa_{33}$ vs the number of points \mathcal{N} used to sample the BZ.

\mathcal{N}	$(\kappa_{33}-\kappa_{11})/\kappa_{33}$
2 304	0.05
4 400	0.03
7 488	0.013
11 760	0.006

of the multiple integral in (46) must be independent of the system of coordinates used to describe the integration domain: nevertheless, errors introduced by the use of a finite number of points are expected to engendre a difference between the numerical value of κ_{33} and that of the two other diagonal components. The magnitude of this difference represents an important tool to judge the reliability of our sampling of the BZ. From Table III, where the ratio $(\kappa_{33}-\kappa_{11})/\kappa_{33}$ is brought vs the number of points, we deduce that our previous choice $\mathcal{N}=7488$ is fully satisfactory, the above ratio being of the order of 10^{-2} and, consequently, lower than the uncertainties affecting the experimental values of κ .

In Figs. 4 and 5 we give κ as a function of temperature at room pressure for solid argon and krypton, and compare the theoretical curve (full line) with experimental data from literature.¹⁰⁻¹⁴ The agreement turns out to be particularly good if one makes reference to the recent data of Kostantinov, Manzhely, Strzhemechnyi, and Smirnov (KMSS),¹⁴ as also shown in a numerical form by Table IV. The rise of κ for $T \rightarrow 0$ is obviously unrealistic, and depends on the circumstance that no boundary scattering has been considered in the present theory. Figures 6 and 7 refer to solid argon and give κ as a function of the molar volume at $T=75$ K, and the ratio $10^2 W/T$ vs T at constant molar volume (22.53 ml), $W=1/\kappa$ being the thermal resistivity: in both cases the agreement between theoretical and experimental data^{15,16} is quite satisfactory and its meaning is enhanced by a comparison with the theory of Julian.¹⁷

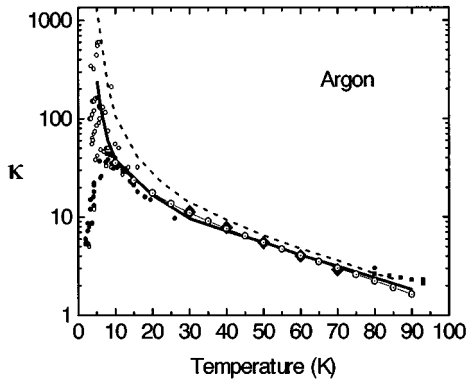


FIG. 4. Thermal conductivity (in $\text{mW cm}^{-1} \text{K}^{-1}$) for argon as a function of temperature at room pressure, as resulting from the present theoretical calculation (continuous line) in comparison with the existing experimental data (\blacksquare , Ref. 10; \circ , Ref. 11; \bullet , Ref. 12; \blacklozenge , Ref. 13; and \odot , Ref. 14) and with the curve obtained by means of the isotropic model (dashed line).

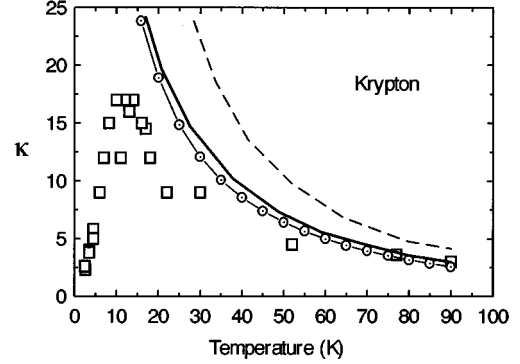


FIG. 5. Thermal conductivity (in $\text{mW cm}^{-1} \text{K}^{-1}$) for krypton as a function of temperature at room pressure, as resulting from the present theoretical calculation (continuous line) in comparison with the prediction of the isotropic model (dashed line) and with the experimental data of White and Woods (Ref. 12) (\square) and of KMSS (Ref. 14) (\odot).

Finally, as in I, we find it interesting to apply our method of solution to an ideal case where all umklapp processes are switched off, and phonon transport is determined by N processes alone. Such a situation can be achieved by multiplying each term with $\nu \geq 1$ in Eqs. (40) and (41) by a factor η smaller than unity and investigating the behavior of κ for $\eta \rightarrow 0$. In this way umklapp collisions (which are exactly described by terms of this kind) are progressively extinguished and an emerging role is attributed to normal collisions (terms with $\nu=0$). The diagram of κ vs η (for Ar at 80 K) is given in Fig. 8 and shows that κ becomes infinitely high for $\eta \rightarrow 0$. This is in agreement with the basic requirement of any theory of thermal conductivity, since normal collisions (in a perfect crystal without boundary effects or isotopic scattering) do not change the total momentum of the phonon system, and consequently cannot be responsible for any resistance to the thermal flux. We find that the above condition is automatically fulfilled by our theory, and corresponds to the fact that the iteration process does not converge for $\eta=0$.

V. CONCLUSIONS

The present paper can be considered as an attempt to calculate, without model approximations, the contribution of three phonon interactions to the thermal resistivity of rare-gas solids: the important work of Benin¹⁸ on a variational

TABLE IV. Comparison of the results obtained by the present theory and by the isotropic model (Ref. 1) with the experimental data of KMSS (Ref. 14) and of White and Woods (WW) (Ref. 12) for argon and krypton. Thermal conductivity is given in $\text{mW}/(\text{cm K})$.

Solid	T (K)	Present			
		theory	Isotropic model	KMSS data	WW data
Ar	80	2.36	2.78	2.3	3.0 ± 0.4
	20	16.6	27.2	17.0	17.0
Kr	80	3.55	4.8	3.16	3.6 ± 0.4
	20	19.3	33.7	18.9	9–12

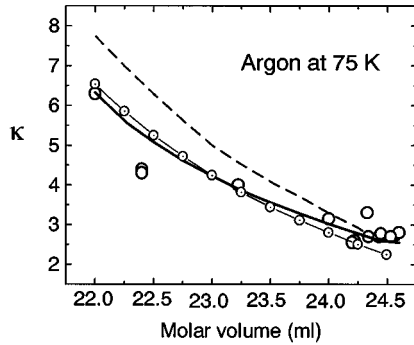


FIG. 6. Thermal conductivity (in $\text{mW cm}^{-1} \text{K}^{-1}$) of argon as a function of the molar volume at 75 K (continuous line) in comparison with the prediction of the isotropic model (dashed line) and with the experimental data of Batchelder (Ref. 15) (\circ) and of KMSS (Ref. 14) (\odot).

calculation of the thermal conductivity of solid argon led to numerical results which were unavoidably affected by the uncertainties connected with the use of the Debye model.

In principle, the knowledge of the three-phonon contribution to the thermal resistivity allows one to deduce, by subtraction from the experimental value, information on other contributions like those due to isotope and impurity scattering, four-phonon processes, etc. First of all, a comparison between our theoretical results and the recent experimental values of κ obtained by KMSS (Ref. 14) shows that the agreement is quite good for argon, while for krypton our conductivity at 80 K and room pressure is about 10% higher than the experimental value. A possible explanation is just provided by isotope scattering, which has not been considered in the present paper: actually, the role of such an effect is expected to be much more relevant in krypton than in argon, according to the table of isotopic abundances given by Ziman² (p. 311). In the absence of a detailed calculation on this point, which is left to a future work, we are in a position

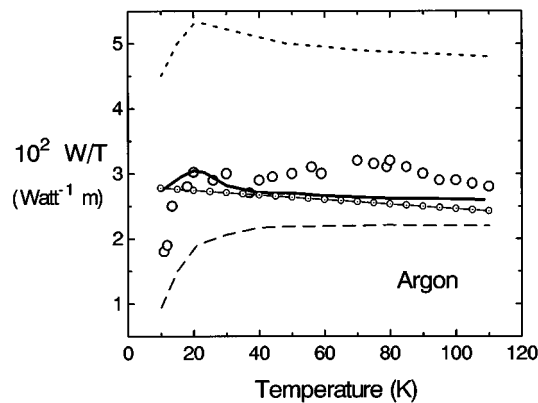


FIG. 7. Temperature dependence of WT^{-1} (thermal resistivity divided by temperature) at fixed molar volume (22.53 ml). The present theory (continuous line) is compared with the experimental data of Clayton and Batchelder (Ref. 16) (\circ) and the experimental data of KMSS (Ref. 14) (\odot) and with the calculation performed in I by means of the isotropic model (dashed line). Also shown is the behavior predicted by Julian (Ref. 17) (dotted line).

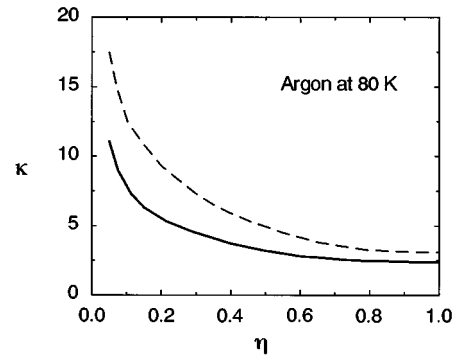


FIG. 8. Thermal conductivity (in $\text{mW cm}^{-1} \text{K}^{-1}$) for argon at 80 K, as a function of the parameter η weighting umklapp collisions (see text): the continuous line refers to the present theory and the dashed line to the isotropic model (Ref. 1).

to conclude that, at least for argon, little space is left for four- or five-phonon contributions to the thermal resistivity.^{19,20} At high temperatures, where these high-order anharmonic contributions should be more effective, the discrepancy between the three-phonon contributions and the observed values of W for argon is probably within the experimental uncertainties (see Fig. 7), so that we have here an indirect proof of the result obtained by Ecsedy and Klemens²¹ about the negligible role played by four-phonon processes. This amounts to saying that, if the discrepancy between KMSS data¹⁴ and Clayton and Batchelder's data¹⁶ is taken as a measure of the experimental uncertainties, there is no experimental evidence of a significant deviation from the $\kappa \propto 1/T$ law predicted at fixed volume by three-phonon interactions: such interactions, therefore, as already pointed out by Batchelder,¹⁵ appear to be fully sufficient to explain the numerical values of thermal conductivity, so that the basic mechanism of heat transport in argon is precisely that suggested a long time ago by Peierls,²² Klemens,²³ and Ziman.² Only if a physical meaning is attributed to the small decrease of W/T observed by KMSS at fixed volume, some supplementary mechanism has to be invoked: this, however, could not be ascribed to four- or five-phonon scattering processes (expected to produce an increase of W/T), but ought to be sought, as suggested by KMSS, in the anharmonic renormalization of phonon-dispersion curves. Of course, the use of such renormalized curves before carrying the iterations would further increase the complexity of our numerical calculations: in the absence of a definite experimental evidence, any reformulation of the present theory in this direction appears to be unreasonable.

A final comment concerns the nearest-neighbor approximation which is usually adopted to describe the anharmonic interactions:⁶ as shown by Fig. 2, the thermal conductivity of solid argon at 80 K, as deducible under the above assumption ($2.73 \text{ mW cm}^{-1} \text{K}^{-1}$) exceeds by about 15% the value calculated by extending the interaction to all the neighbors ($2.36 \text{ mW cm}^{-1} \text{K}^{-1}$). Such a result means that any calculation of thermal conductivity based on the above approximation is affected by errors decidedly larger than the experimental uncertainties (at least at high temperatures) and this should be particularly true for ionic crystals, owing to the long range of the Coulomb interaction.

- ¹M. Omini and A. Sparavigna, *Physica B* **212**, 101 (1995).
- ²J. M. Ziman, *Electrons and Phonons* (Clarendon, London, 1962).
- ³G. P. Srivastava, *The Physics of Phonons* (Hilger, Bristol, 1990).
- ⁴R. A. H. Hamilton and J. E. Parrott, *Phys. Rev.* **178**, 1284 (1969).
- ⁵M. Omini and A. Sparavigna, *Philos. Mag. B* **68**, 767 (1993).
- ⁶S. Pettersson, *J. Phys. C* **20**, 1047 (1987).
- ⁷R. N. Gurzhi, *Sov. Phys. Usp.* **11**, 255 (1968).
- ⁸V. L. Gurevich, *Transport in Phonon Systems* (North-Holland, Amsterdam, 1986).
- ⁹D. C. Wallace, *Thermodynamics of Crystals* (Wiley, New York, 1972).
- ¹⁰B. J. Bailey and K. Kellner, *Physica* **39**, 444 (1968).
- ¹¹A. Bernè, G. Boato, and M. De Paz, *Nuovo Cimento* **46**, 182 (1966).
- ¹²G. K. White and S. B. Woods, *Philos. Mag.* **3**, 785 (1958).
- ¹³I. N. Krupskii and V. G. Manzhely, *Phys. Status Solidi* **24**, K53 (1967).
- ¹⁴V. A. Kostantinov, V. G. Manzhely, M. A. Strzhemechnyi, and S. A. Smirnov, *Sov. J. Low Temp. Phys.* **14**, 48 (1988).
- ¹⁵D. N. Batchelder, in *Rare Gas Solids*, edited by M. L. Klein and J. A. Vanables (Academic, London, 1977), Vol. 2.
- ¹⁶F. Clayton and D. N. Batchelder, *J. Phys. C* **6**, 1213 (1973).
- ¹⁷C. L. Julian, *Phys. Rev.* **137**, A128 (1965).
- ¹⁸D. B. Benin, *Phys. Rev. B* **1**, 2777 (1970).
- ¹⁹Y. P. Joshi, M. D. Tiwari, and G. S. Verma, *Phys. Rev.* **139**, 642 (1970).
- ²⁰B. D. Indu and R. P. Gairola, *Indian J. Theor. Phys.* **33**, 115 (1990).
- ²¹D. J. Ecsedi and P. G. Klemens, *Phys. Rev. B* **15**, 5957 (1977).
- ²²R. Peierls, *Ann. Phys.* **3**, 1005 (1929).
- ²³P. G. Klemens, in *Solid State Physics: Advances in Research and Applications*, edited by F. Seitz and D. Turnbull (Academic, New York, 1958), Vol. 7, p. 1.